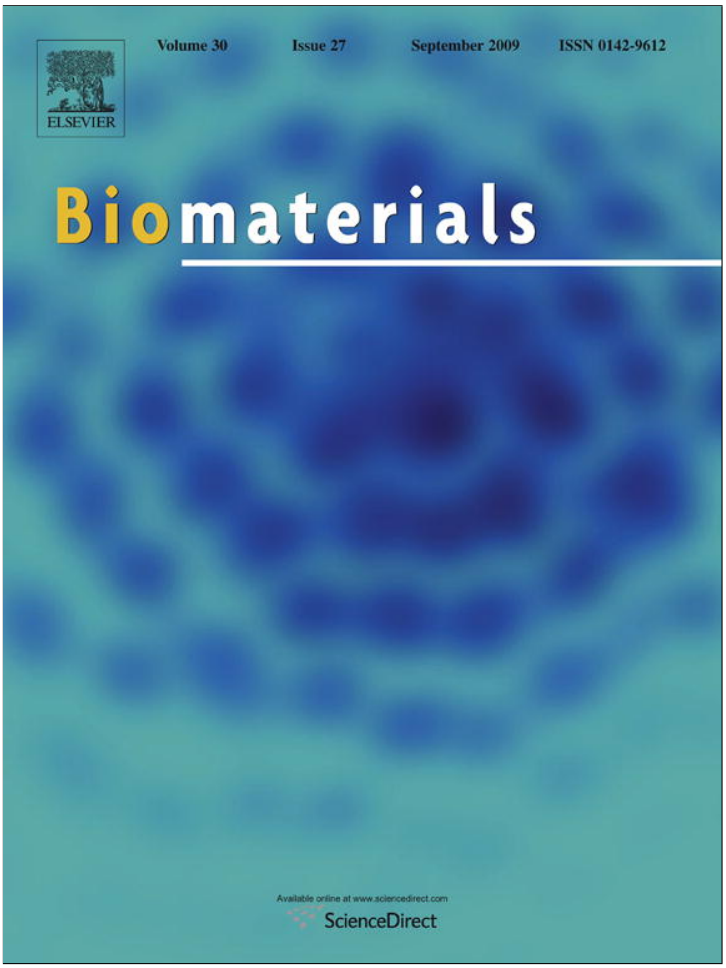

Biomaterials 30 (2009) 4488–4493

Contents lists available at ScienceDirect

Biomaterials

journal homepage: www.elsevier.com/locate/biomaterials

Randomly oriented, upright SiO_2 coated nanorods for reduced adhesion of mammalian cells

Jiyeon Lee, Byung Hwan Chu, Ke-Hung Chen, Fan Ren, Tanmay P. Lele*

Department of Chemical Engineering, University of Florida, Gainesville, FL 32611, USA

ARTICLE INFO

Article history:
Received 6 March 2009
Accepted 10 May 2009
Available online 10 June 2009

Keywords:
Nanorods
Cell adhesion
Cell survival
Anti-fouling

ABSTRACT

Cell interactions with nanostructures are of broad interest because of applications in controlling tissue response to biomedical implants. Here we show that dense and upright SiO_2 coated nanorods nearly eliminate cell adhesion in fibroblasts and endothelial cells. The lack of adhesion is not due to a decrease in matrix protein adsorption on the nanostructures, but rather an inability of cells to assemble focal adhesions. Using spatially patterned nanorods, we show that cells display a preference for flat regions of the surface. Our results support a model in which interfering with nanoscale spacing of ligated integrins results in reduced cell adhesion and subsequent cell death. We propose that dense monolayers of nanorods are a promising nanotechnology for preventing mammalian cell fouling of biomaterials.

Published by Elsevier Ltd.

1. Introduction

Anchorage-dependent cells need to attach and spread on solid surfaces for normal function [1–3]. Modulating cell adhesion and survival by tailoring the surface is a promising strategy that has applications in tissue engineering and biomedical implants [4–7]. Cell adhesion to surfaces involves the adhesion of integrin receptors to their ligands, followed by subsequent nanoscale clustering of ligated integrins [8,9]. Therefore, recent approaches to modulate cell adhesion have focused on controlling the nanoscale adhesion and clustering of integrins [8–15]. These approaches include spatially patterning adhesive ligands [8–11], modulating the nanotopography of the substrate [12–15], surface modification with biocompatible polymers [16,17], and controlling cell attachment on patterned structures [18–20]. Applications for controlling cell behavior with nanostructured and nanopatterned materials range from improving integration of titanium implants with bone [21,22], to developing polymer scaffolds that better mimic the extracellular matrix [7,23], to anti-fouling materials for preventing cell adhesion to biomedical implants [24–26]. In particular, the design of effective surfaces that prevent mammalian cell adhesion has remained a fundamental challenge [27].

There are relatively few studies that have explored the use of nanostructures for eliminating mammalian cell adhesion and survival. Some evidence suggests that nanostructured materials can be developed to reduce protein adsorption [28–30] and to potentially decrease cell adhesion [13–15,31]. In a previous paper, we have shown that endothelial cells and fibroblasts are unable to adhere and survive on zinc oxide (ZnO) nanorods compared to flat ZnO substrates [13]. The advantage of ZnO nanorods is that they can be grown with solution-based crystallization techniques at low-temperature. Thus, the nanorods can be coated on surfaces of irregular geometries, and temperature sensitive materials such as stents. However, it is unclear if the dramatic decrease in cell adhesion and survival observed on ZnO nanorods is reproducible with similar nanorods but of a different material. The chemical nature of the nanorod surface is clearly important given that it can potentially influence protein adsorption. In addition, ZnO has the potential for having long-term toxicity to cells due to leaching into solution [32–34].

Silicon dioxide (SiO_2) based nanowires and nanoneedles have received recent attention for modulating cell adhesion [15,35]. Previous studies have shown that stem cells can survive for long periods of time on surfaces sparsely coated with SiO_2 nanowires [35]. Conversely, on comparatively denser SiO_2 nanoneedles, cell adhesion is decreased, suggesting their potential for anti-fouling surfaces [15]. However, the decrease in cell adhesion on nanoneedles was not observed to be as dramatic [15] as previously reported with ZnO nanorods [13].

Therefore, in this paper, we explored if SiO_2 nanorods with similar morphologies as the previously used ZnO nanorods can result in a similar dramatic decrease in mammalian cell adhesion and survival. Our observations provide further evidence that densely packed upright nanorods can be used to develop surfaces resistive to mammalian cell adhesion.

* Corresponding author. Tel.: +1 352 392 0317; fax: +1 352 392 9513.
E-mail address: tlele@che.ufl.edu (T.P. Lele).

0142-9612/$ – see front matter Published by Elsevier Ltd.
doi:10.1016/j.biomaterials.2009.05.028

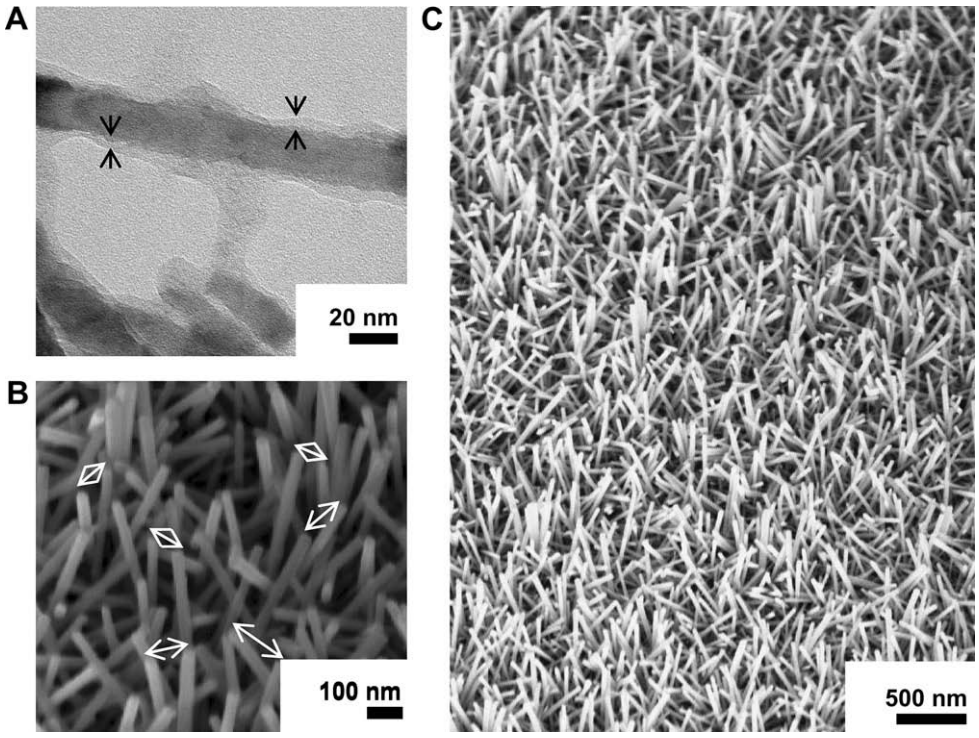

Fig. 1. The morphology of nanorods. (A) TEM image of SiO_2 deposited ZnO nanorods. Black arrows indicate SiO_2 thin film with a 50 Å thickness. ZnO nanorods are encapsulated by SiO_2. (B) Scanning electron microscopy (SEM) image of nanorods on glass. White arrows indicate the spacing between nanorods. The spacing between nanorods ranges from 80 to 100 nm. (C) SEM image of a monolayer of nanorods. Upright nanorods were covered on the underlying glass substrate uniformly.

2. Materials and methods

2.1. Fabrication of nanorods

ZnO nanorods were made by a solution-based hydrothermal growth method [36]. First, ZnO nanocrystal seed solutions were prepared by mixing 15 mM zinc acetate dihydrate (Sigma Aldrich, St. Louis, MO) with 30 mM of NaOH (Sigma Aldrich, St. Louis, MO) at 60 °C for 2 h. Next, ZnO nanocrystals were spin-coated onto the substrate and then post-baked on a hot plate at 200 °C for better adhesion. The substrate with these seeds was then suspended upside down in a Pyrex glass dish filled with an aqueous nutrient solution. The growth rate was approximately 1 μm per hour with 100 ml aqueous solution containing 20 mM zinc nitrate hexahydrate and 20 mM hexamethylenetriamine (Sigma Aldrich, St. Louis, MO). To arrest the nanorod growth, the substrates were removed from solution, rinsed with de-ionized water and dried in air at room temperature. SiO_2 was deposited with a Unaxis 790 plasma enhanced chemical vapor deposition (PECVD) system at 50 °C using N_2O and 2% SiH_4 balanced by nitrogen as the precursors as reported before [37]. Patterned nanorods were fabricated by conventional photoresist (PR) lithography [36]. A glass slide was processed with negative PR (SU-8 2007, Microchem) so that a pattern with 50 μm circles was formed on the surface. The substrate was then post-baked at 110 °C for 30 min. The processed substrate was spin-coated with ZnO nanocrystals as seed materials and nanorods were grown on the substrate with an aqueous nutrient solution. The negative PR was removed by PG remover in a warm bath at 60 °C for 30 min. Patterned nanorods were also coated with SiO_2.

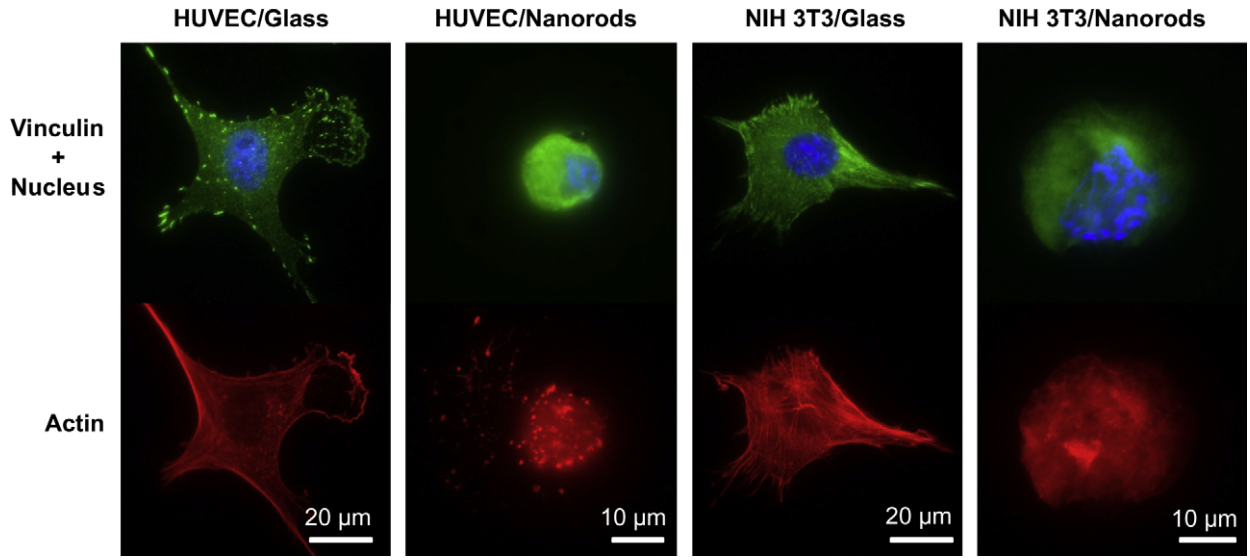

Fig. 2. Fluorescent microscopic images of HUVEC and NIH 3T3 on glass and nanorods. HUVEC and NIH 3T3 on glass assemble focal adhesions stained with vinculin (green) and actin stress fibers (red). Nuclei were stained with DAPI (blue). HUVEC and NIH 3T3 on nanorods are unable to spread and assemble focal adhesions and stress fibers.

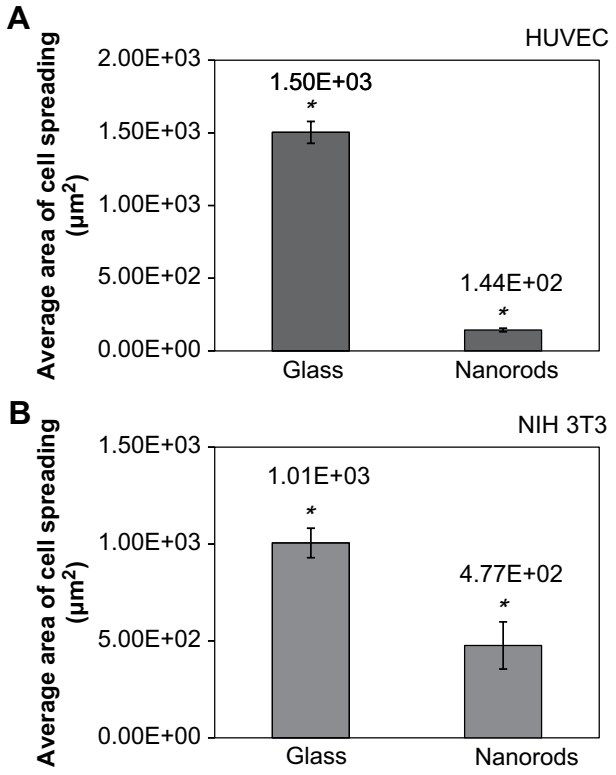

Fig. 3. The average area of cell spreading on glass and nanorods. (A) HUVEC on glass and nanorods ($n > 170$). (B) NIH 3T3 on glass and nanorods ($n > 110$). * indicates $p < 0.005$. Spreading area is significantly decreased on nanorods compared to glass. Bar indicates standard error of the mean (SEM). The data were pooled from three independent experiments.

2.2. Contact angle measurements

The contact angle of de-ionized water with surfaces was measured with a Ramé-Hart Goniometer and Ramé-Hart DROPimage Advanced Software using the sessile drop technique.

2.3. Cell culture

For control substrate 22 mm square glass cover slips were used (Corning, Inc., Lowell, MA). Before use, each substrate was sterilized with UV for 5 min and cleaned in 70% ethanol and de-ionized water. After drying substrates in air at room temperature, they were treated with 5 μg/ml human fibronectin (FN) (BD biosciences, Bedford, MA). After overnight incubation with FN at 4 °C, the substrates were washed twice with PBS. NIH 3T3 fibroblasts were cultured in DMEM (Mediatech, Inc., Herndon, VA) supplemented with 10% donor bovine serum (DBS) (Hyclone, Logan, UT). Human umbilical cord vein endothelial cells (HUVECs) were cultured in EBM-2 Basal Medium and EGM-2 Single Quot Kit (Lonza, Walkersville, MD). Cell suspensions of the same concentration and volume (i.e. same number of cells) were then seeded on each substrate.

2.4. Immunostaining and cell viability assay

After 24 h of cell seeding, non-adherent cells were removed with two gentle washes with PBS. The samples were fixed with 4% paraformaldehyde for 20 min and washed several times with PBS. Fixed cells were immuno-stained for vinculin and stained for actin and nucleus using our previously reported methods [13]. Briefly, cells were fixed with 4% paraformaldehyde, permeabilized with 0.2% Triton X-100, and treated with mouse monoclonal anti-vinculin antibody (Sigma Aldrich, St. Louis, MO), followed by goat anti-mouse secondary antibody conjugated with Alexa Fluor 488 (Invitrogen, Eugene, OR). Actin was stained with phalloidin conjugated with Alexa Fluor 594 (Invitrogen, Eugene, OR) and nucleus was stained with 4′-6-diamidino-2-phenylindole (DAPI) (Sigma Aldrich, St. Louis, MO). Cells were then imaged on a Nikon TE 2000 epifluorescence microscope using GFP, Texas Red and DAPI filters. All images were collected using the NIS-Elements program (Nikon).

The live/dead viability/cytotoxicity kit for mammalian cells (Invitrogen, Eugene, OR) was used for quantifying adherent cell viability on each substrate. Cells were incubated at 30–45 min with calcein AM (2 μM for fibroblast and 4 μM for endothelial cells) and ethidium homodimer-1 (EthD-1) (4 μM for all types of the cells). Next, epifluorescence images of six to ten random fields were collected on a Nikon TE 2000 inverted microscope using a 10× lens for NIH 3T3 and HUVEC. The average number of cells adherent on each substrate, the number of adherent live cells (stained green with calcein AM) and adherent dead cells (stained red with EthD-1) were quantified from these images using the NIS-Elements program (Nikon). Three independent experiments of cell viability were performed and the data were pooled. The average area of cell spreading was determined from three independent experiments with statistical comparison using Student's *T*-test.

2.5. Time lapse imaging

Cells were pre-cultured on the patterned nanorods for 24 h as mentioned above. Before imaging, non-adherent cells were removed with two gentle washes with PBS and new media was added to the dish. Phase contrast imaging was performed for 6 h on the Nikon TE 2000 microscope with humidified incubator (In Vivo Scientific, St. Louis, MO). Images were collected every 5 min using a 10× objective.

2.6. Protein adsorption on nanorods and glass

Sterilized SiO_2 coated nanorod and glass substrates were prepared as outlined above. Both of the substrates were incubated with 10 μg/ml rhodamine fibronectin (Cytoskeleton, CO) diluted in PBS overnight and these dishes were washed with PBS several times. Five randomly taken 20× fluorescent images were collected with identical illumination and exposure time, and the fluorescent intensity was analyzed by the NIS-Element program (Nikon).

3. Results and discussion

3.1. Fabrication of SiO_2 coated nanorods

Many biomedical implants are made of temperature sensitive materials such as plastic. Hence, it is necessary to grow nanorods with techniques that do not require high temperature. Densely packed ZnO nanorods were fabricated with a low-temperature (95 °C) hydrothermal, solution-based growth method [36]. We next deposited nano-thin films of SiO_2 with controlled thickness, 50 Å, using PECVD at 50 °C according to our previously published methods [37]. Transmission electron microscopy (TEM) images of the resulting nanorods with 50 Å thickness of SiO_2 nano-films deposited are shown in Fig. 1A. The nanorods were randomly oriented in the upright direction, approximately 40–50 nm in diameter, 500 nm in height. The average spacing between nanorods was approximately 80–100 nm (Fig. 1A, white arrows). Importantly, the SiO_2 coatings were deposited uniformly on each nanorod free of any local defects, which was confirmed with TEM, local electrical conductance measurements, chemical wet-etching and photoluminescence

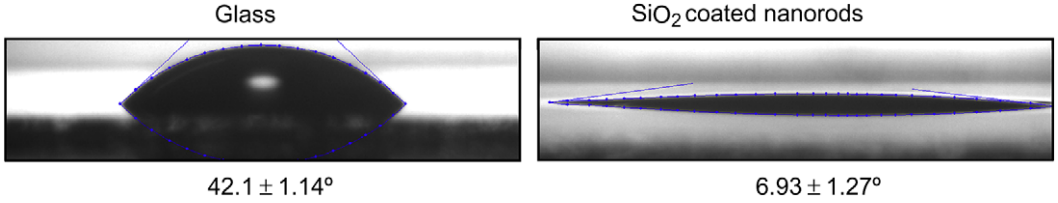

Fig. 4. Contact angles of water on glass and SiO_2 coated nanorods. The SiO_2 coated nanorod surface was hydrophilic, with average contact angle of 6.93+/−1.27° compared to glass of contact angle 42.1+/−1.14°. Error indicates the standard deviation (SD).

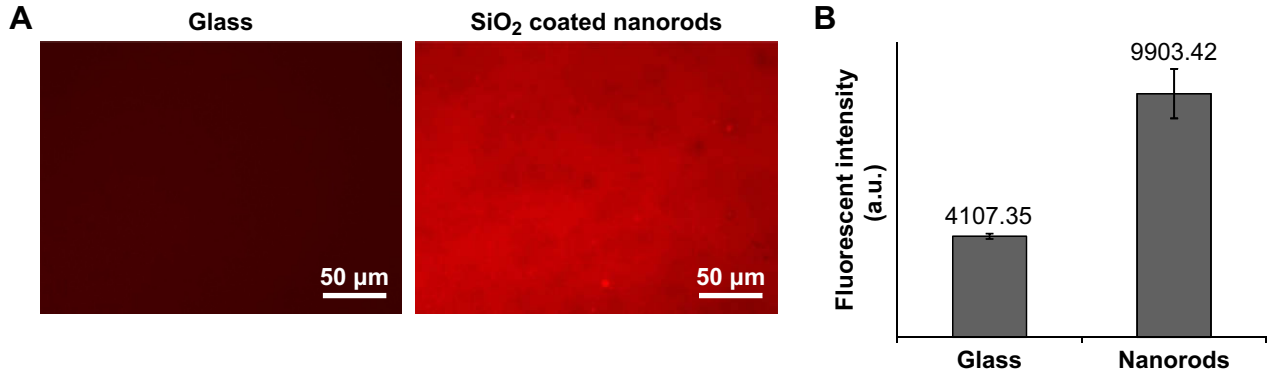

Fig. 5. Fluorescent images and intensity of rhodamine fibronectin coated glass and nanorods. (A) Representative fluorescent images of rhodamine fibronectin on glass and SiO_2 coated nanorods. (B) Plots show the average intensity profile pooled from five randomly taken images. Fibronectin adsorption is increased two-fold on nanorods compared to glass. Bar indicates SD.

intensity measurements [37]. Our technique thus resulted in randomly oriented, upright SiO_2 deposited nanorods that cover the surface with densely packed monolayers without any defects over cm length scales (Fig. 1C).

3.2. Decreased cell adhesion on SiO_2 coated nanorods

Cell adhesion and spreading occurs by the ligation of transmembrane integrins to ligands (such as fibronectin) immobilized on the surface. This is followed by clustering of the integrins at the nanoscale, and subsequent formation of multi-protein, micron-scale assemblies called focal adhesions [38]. Focal adhesions allow force transfer from the contractile acto-myosin cytoskeleton inside the cell to the outside surface, and this allows cells to adhere to and spread on the surface. If focal adhesions are not allowed to assemble in cells that depend on anchorage for survival, this leads to weak attachment to the surface, lack of cell spreading and subsequent apoptosis [39,40]. Therefore, the assembly of focal adhesions was next studied using immunofluorescence microscopy.

Human umbilical vein endothelial cells (HUVECs) and NIH 3T3 fibroblasts were cultured on SiO_2 nanorods which were pre-incubated with fibronectin overnight. Cells were fixed with paraformaldehyde and stained for vinculin, actin stress fibers and the nucleus. Both HUVECs and NIH 3T3 fibroblasts assembled vinculin-labeled focal adhesions on glass (Fig. 2). On the nanorod-coated surfaces, focal adhesions were not visible and cells were rounded and poorly spread (Fig. 2). Cells on nanorods were also unable to assemble contractile stress fibers. Consequently, the average area of cell spreading on nanorods was significantly decreased (Fig. 3) with a lack of focal adhesion and stress fiber formation. This result suggests that cells are unable to spread and assemble focal adhesions on nanorods, which may cause apoptosis in these adhesion-dependent cells [39,40].

3.3. Protein adsorption on nanorods

Recent work by Spatz and co-workers showed that focal adhesion assembly requires the spacing between ligated integrins to be less than 70 nm [8,9]. A spacing of more than 73 nm between ligated integrins limits attachment, spreading, and actin stress fiber formation in fibroblasts. As the diameter of the SiO_2 nanorods is approximately 40–50 nm, local integrin clustering may occur but to a very limited extent given the vertical nature and small length (500 nm) of the nanorods. Due to the spacing of 80–100 nm, integrin clustering may not occur over multiple nanorods, preventing the assembly of contiguous focal adhesions on the micron length scale (Fig. 2).

Other possible explanations for the fact that cells cannot spread on nanorods are the super-hydrophobic nature of nanostructured surfaces such as ZnO nanorods [31,41]. Protein adsorption is decreased on super-hydrophobic surfaces which potentially can explain decreased adhesion. To address this question, we measured contact angles of SiO_2 coated nanorods. We found that SiO_2 coated nanorods were hydrophilic (Fig. 4: contact angle of $6.93+/-1.27^\circ$ compared to glass of $42.1+/-1.14^\circ$). As fibronectin is known to adsorb successfully on hydrophilic surfaces [42], this result suggests that reduced matrix protein adsorption is likely not the reason for decreased adhesion.

To confirm this, we next measured the extent of fibronectin adsorption on nanorods (Fig. 5). Rhodamine-labeled fibronectin was deposited overnight on SiO_2 coated nanorods and flat glass

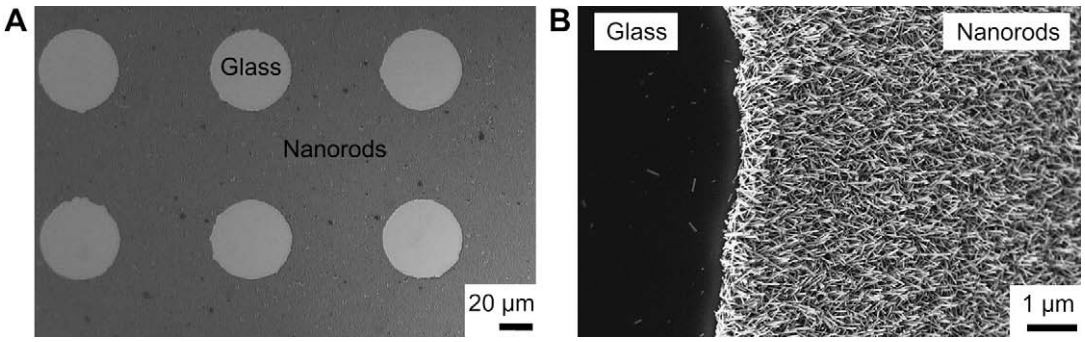

Fig. 6. SEM images of patterned nanorods. (A) Optical microscope image with 400× objective. (B) SEM image.

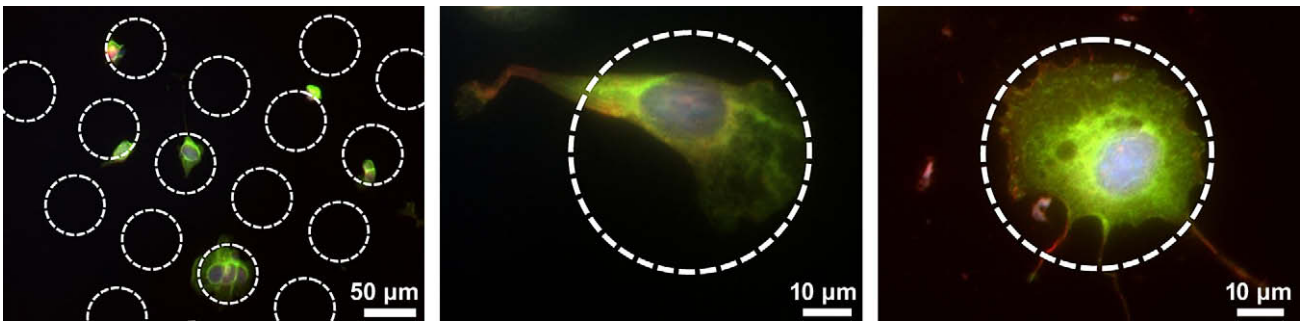

Fig. 7. NIH 3T3 fibroblasts on patterned SiO_2 coated nanorods. Fluorescent microscopic images showing that NIH 3T3 fibroblasts preferably attached on glass. Cells are stained for actin (red), vinculin (green) and nucleus (blue). Cells were confined on the flat circular regions. Dashed lines indicate the edge of patterns.

substrates. Fluorescent images of the rhodamine fibronectin adsorbed surface were captured and analyzed for differences in intensity. Interestingly, we found that fibronectin adsorption as measured by fluorescence intensity was increased two-fold on SiO_2 coated nanorods compared to glass. An increase in protein adsorption is to be expected given the increased surface area of the nanorods. The increase in fibronectin adsorption argues against large decreases in protein adsorption as being responsible for the observed reduction in cell adhesion. Importantly, fibronectin is known to adsorb in an active conformation on hydrophilic surfaces [42]. Given that all our experiments were carried out in 10% serum which allows the adsorption of other matrix proteins on the hydrophilic surface, and also promotes the secretion of fibronectin by the cells themselves, it is unlikely that decreased or abnormal matrix protein adsorption plays a significant role in the observed response.

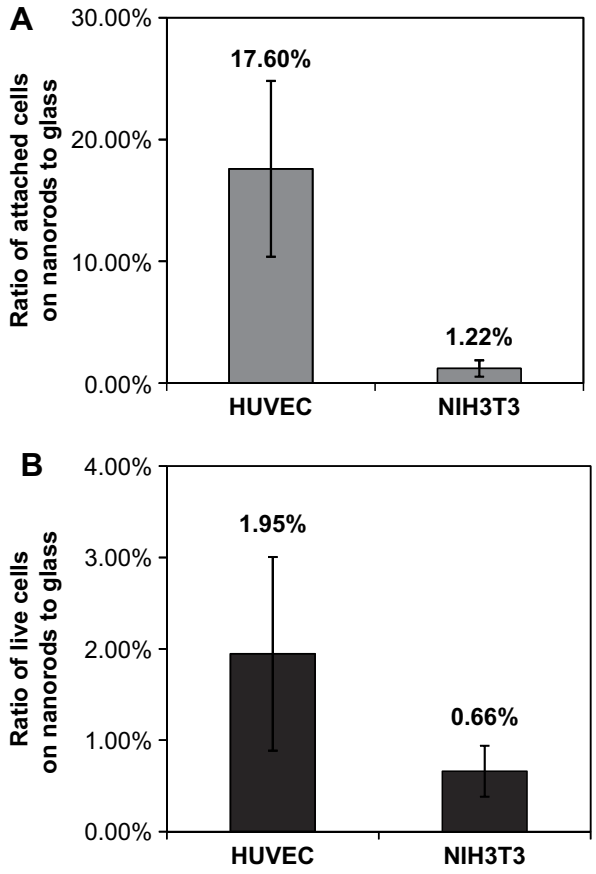

Fig. 8. Cell attachment and viability on nanorods. (A) The ratio of the number of attached cells on nanorods to that on glass. (B) The ratio of the number of live cells on nanorods to that on glass. ($n > 2500$ for HUVECs, $n > 1500$) for NIH 3T3. Cells are considerably reduced in numbers on nanorods. Bar indicates SEM.

3.4. Spatial patterning of cell adhesion with nanorods

To investigate if it is feasible to pattern cell adhesion with nanorods, we spatially patterned nanorods using a low-temperature, and patterned growth method [36]. This method results in patterned nanorods that are not present inside circles, and are present outside in dense monolayers (Fig. 6). The diameter of circles was 50 μm and spacing between the circles was 40–60 μm. Nanorods were 50 nm in diameter and 500 nm in height. Fig. 7A and B shows that fibroblasts preferably adhered to the flat surface rather than to the nanorods after 48 h culture. Similar patterning was also observed with ZnO nanorods without SiO_2 coating (Fig. 1S in the supplementary information). Moreover, while the cells were confined to the circular regions on average, cells were frequently able to migrate from circle to circle by spanning the intervening nanorods (see Fig. 2S, and Movies 1S and 2S for an example of cell migration on patterned ZnO nanorods). This result suggests that spatially patterned nanorods provide a new way of dynamically patterning cells and therefore creating complex tissues.

3.5. Decreased cell survival on nanorods

The number of cells adherent on SiO_2 coated nanorods was significantly reduced (a reduction of 98% in fibroblasts, 82% in HUVECs) compared to cells on glass (Fig. 8A) after 24 h culture. Next, a live/dead viability/cytotoxicity kit for mammalian cells was used for quantifying adherent cell viability. The decrease in viability in cells on nanorods compared to that on glass was dramatic (Fig. 8B) with only one or two cells surviving on the SiO_2 nanorods for every 100 viable cells on glass. By culturing cells on glass in media that was incubated for 1 day, 3 days and 7 days with the nanorods, we confirmed that the cell death was not due to toxicity of unknown dissolving material from the nanorods (see Fig. 3S in the supplementary information). Therefore, these results suggest that densely packed nanorods have excellent anti-fouling potential by virtue of their topology.

4. Conclusion

Our results indicate that dense nanorod coatings are a powerful approach to eliminate cell adhesion and viability in anchorage-dependent cells, and a novel strategy for achieving anti-fouling. The mechanism is likely to be due to the lack of integrin clustering at the nanoscale.

Acknowledgements

We thank Dr. Chih-Yang Chang for analyzing SEM image and Lii-Cherng Leu for taking TEM image. This work was partially supported by a grant from the American Heart Association (0735203N) to TPL.

Appendix

Figures with essential colour discrimination. Certain figures in this article, in particular parts of Figs. 2, 5 and 7 are difficult to interpret in black and white. The full colour images can be found in the on-line version, at doi:10.1016/j.biomaterials.2009.05.028.

Appendix. Supplementary information

Supplementary material associated with this article can be found in the on-line version at doi:10.1016/j.biomaterials.2009.05.028.

References

[1] Benzeev A, Farmer SR, Penman S. Protein-synthesis requires cell–surface contact while nuclear events respond to cell-shape in anchorage-dependent fibroblasts. Cell 1980;21:365–72.
[2] Ingber DE. Fibronectin controls capillary endothelial-cell growth by modulating cell-shape. Proc Natl Acad Sci U S A 1990;87:3579–83.
[3] Mooney D, Hansen L, Vacanti J, Langer R, Farmer S, Ingber D. Switching from differentiation to growth in hepatocytes – control by extracellular-matrix. J Cell Physiol 1992;151:497–505.
[4] Park H, Cannizzaro C, Vunjak-Novakovic G, Langer R, Vacanti CA, Farokhzad OC. Nanofabrication and microfabrication of functional materials for tissue engineering. Tissue Eng 2007;13:1867–77.
[5] Goldberg M, Langer R, Jia XQ. Nanostructured materials for applications in drug delivery and tissue engineering. J Biomater Sci Polym Ed 2007;18:241–68.
[6] Ainslie KM, Desai TA. Microfabricated implants for applications in therapeutic delivery, tissue engineering, and biosensing. Lab Chip 2008;8:1864–78.
[7] Ma ZW, He W, Yong T, Ramakrishna S. Grafting of gelatin on electrospun poly(caprolactone) nanofibers to improve endothelial cell spreading and proliferation and to control cell orientation. Tissue Eng 2005;11:1149–58.
[8] Arnold M, Cavalcanti-Adam EA, Glass R, Blummel J, Eck W, Kantlehner M, et al. Activation of integrin function by nanopatterned adhesive interfaces. Chem Phys Chem 2004;5:383–8.
[9] Girard PP, Cavalcanti-Adam EA, Kemkemer R, Spatz JP. Cellular chemomechanics at interfaces: sensing, integration and response. Soft Matter 2007;3:307–26.
[10] Dillmore WS, Yousaf MN, Mrksich M. A photochemical method for patterning the immobilization of ligands and cells to self-assembled monolayers. Langmuir 2004;20:7223–31.
[11] Petty RT, Li HW, Maduram JH, Ismagilov R, Mrksich M. Attachment of cells to islands presenting gradients of adhesion ligands. J Am Chem Soc 2007;129:8966–7.
[12] Park J, Bauer S, von der Mark K, Schmuki P. Nanosize and vitality: TiO_2 nanotube diameter directs cell fate. Nano Lett 2007;7:1686–91.
[13] Lee J, Kang BS, Hicks B, Chancellor TF, Chu BH, Wang HT, et al. The control of cell adhesion and viability by zinc oxide nanorods. Biomaterials 2008;29:3743–9.
[14] Dalby MJ, Riehle MO, Sutherland DS, Agheli H, Curtis AS. Morphological and microarray analysis of human fibroblasts cultured on nanocolumns produced by colloidal lithography. Eur Cell Mater 2005;9:1–8.
[15] Choi CH, Hagvall SH, Wu BM, Dunn JC, Beygui RE, CJK CJ. Cell interaction with three-dimensional sharp-tip nanotopography. Biomaterials 2007;28:1672–9.
[16] Yeo WS, Mrksich M. Electroactive self-assembled monolayers that permit orthogonal control over the adhesion of cells to patterned substrates. Langmuir 2006;22:10816–20.
[17] Sofia SJ, Premnath VV, Merrill EW. Poly(ethylene oxide) grafted to silicon surfaces: grafting density and protein adsorption. Macromolecules 1998;31:5059–70.
[18] Thakar RG, Chown MG, Patel A, Peng L, Kumar S, Desai TA. Contractility-dependent modulation of cell proliferation and adhesion by microscale topographical cues. Small 2008;4:1416–24.
[19] Khademhosseini A, Langer R, Borenstein J, Vacanti JP. Microscale technologies for tissue engineering and biology. Proc Natl Acad Sci U S A 2006;103:2480–7.
[20] Karp JM, Yeh J, Eng G, Fukuda J, Blumling J, Suh KY, et al. Controlling size, shape and homogeneity of embryoid bodies using poly(ethylene glycol) microwells. Lab Chip 2007;7:786–94.
[21] Sato M, Aslani A, Sambito MA, Kalkhoran NM, Slamovich EB, Webster TJ. Nanocrystalline hydroxyapatite/titania coatings on titanium improves osteoblast adhesion. J Biomed Mater Res A 2008;84:265–72.
[22] Puckett S, Pareta R, Webster TJ. Nano rough micron patterned titanium for directing osteoblast morphology and adhesion. Int J Nanomedicine 2008;3:229–41.
[23] Venugopal J, Low S, Choon AT, Ramakrishna S. Interaction of cells and nanofiber scaffolds in tissue engineering. J Biomed Mater Res B Appl Biomater 2008;84:34–48.
[24] Meng J, Meng J, Duan J, Kong H, Li L, Wang C, et al. Carbon nanotubes conjugated to tumor lysate protein enhance the efficacy of an antitumor immunotherapy. Small 2008;4:1364–70.
[25] Tran P, Webster TJ. Enhanced osteoblast adhesion on nanostructured selenium compacts for anti-cancer orthopedic applications. Int J Nanomedicine 2008;3:391–6.
[26] Ratner BD, Hoffman AS, Schoen FJ, Lemmons JE. Biomaterials science: an introduction to materials in medicine. London, UK: Elsevier Academic Press; 2004.
[27] Anderson JM, Rodriguez A, Chang DT. Foreign body reaction to biomaterials. Semin Immunol 2008;20:86–100.
[28] Asuri P, Karajanagi SS, Kane RS, Dordick JS. Polymer-nanotube-enzyme composites as active antifouling films. Small 2007;3:50–3.
[29] Koc Y, de Mello AJ, McHale G, Newton MI, Roach P, Shirtcliffe NJ. Nano-scale superhydrophobicity: suppression of protein adsorption and promotion of flow-induced detachment. Lab Chip 2008;8:582–6.
[30] Ainslie KM, Sharma G, Dyer MA, Grimes CA, Pishko MV. Attenuation of protein adsorption on static and oscillating magnetostrictive nanowires. Nano Lett 2005;5:1852–6.
[31] Sun T, Tan H, Han D, Fu Q, Jiang L. No platelet can adhere – largely improved blood compatibility on nanostructured superhydrophobic surfaces. Small 2005;1:959–63.
[32] Brinkman SF, Johnston WD. Acute toxicity of aqueous copper, cadmium, and zinc to the mayfly *Rhithrogena hageni*. Arch Environ Contam Toxicol 2008;54:466–72.
[33] Lin WS, Xu Y, Huang CC, Ma YF, Shannon KB, Chen DR, et al. Toxicity of nano- and micro-sized ZnO particles in human lung epithelial cells. J Nanopart Res 2009;11:25–39.
[34] Gojova A, Guo B, Kota RS, Rutledge JC, Kennedy IM, Barakat AI. Induction of inflammation in vascular endothelial cells by metal oxide nanoparticles: effect of particle composition. Environ Health Perspect 2007;115:403–9.
[35] Kim W, Ng JK, Kunitake ME, Conklin BR, Yang P. Interfacing silicon nanowires with mammalian cells. J Am Chem Soc 2007;129:7228–9.
[36] Kang BS, Pearton SJ, Ren F. Low temperature (<100 degrees C) patterned growth of ZnO nanorod arrays on Si. Appl Phys Lett 2007;90:084104.
[37] Chu BH, Leu LC, Chang CY, Lugo F, Norton D, Lele T, et al. Conformable coating of SiO_2 on hydrothermally grown ZnO nanorods. Appl Phys Lett 2008;93:233111.
[38] Bershadsky A, Kozlov M, Geiger B. Adhesion-mediated mechanosensitivity: a time to experiment, and a time to theorize. Curr Opin Cell Biol 2006;18:472–81.
[39] Chen CS, Mrksich M, Huang S, Whitesides GM, Ingber DE. Geometric control of cell life and death. Science 1997;276:1425–8.
[40] Re F, Zanetti A, Sironi M, Polentarutti N, Lanfrancone L, Dejana E, et al. Inhibition of anchorage-dependent cell spreading triggers apoptosis in cultured human endothelial cells. J Cell Biol 1994;127:537–46.
[41] Feng X, Feng L, Jin M, Zhai J, Jiang L, Zhu D. Reversible super-hydrophobicity to super-hydrophilicity transition of aligned ZnO nanorod films. J Am Chem Soc 2004;126:62–3.
[42] Grinnell F, Feld MK. Fibronectin adsorption on hydrophilic and hydrophobic surfaces detected by antibody binding and analyzed during cell adhesion in serum-containing medium. J Biol Chem 1982;257:4885–93.